One-channel time-reversal in chaotic cavities: Experimental results

Carsten Draeger,[a] Jean-Christian Aime, and Mathias Fink
Laboratoire Ondes et Acoustique, URA CNRS 1503, Université Paris VII Denis Diderot – Ecole Supérieure de Physique et de Chimie Industrielles de la Ville de Paris, 10 Rue Vauquelin, 75005 Paris, France

(Received 15 December 1997; accepted for publication 5 October 1998)

Experiments are presented that show the feasibility of reconstructing a point source using acoustic time-reversal with a single transmitter/receiver. The propagation medium is a closed 2-D silicon cavity with chaotic ray dynamics and negligible absorption. Injection of a short pulse at one point yields a long signal at a second one; by reversing a part of this signal, we obtain a focus at the initial injection point. The characterization of the focus was observed by scanning with an optical interferometer and by measuring the signal at the focal spot. With circular converging wavefronts, the reconstructed focus was excellent (corresponding to an aperture of 360°), but not perfect. The increase in quality of the focus with growing length of the reversed signal is described by a statistical ray model. Despite the irreversibility in classical chaos (due to strong sensitivity to initial conditions), the underlying chaotic ray dynamics is useful in this case. © *1999 Acoustical Society of America.* [S0001-4966(99)04301-5]

PACS numbers: 43.20.−f, 43.20.Dk, 43.20.Fn, 43.25.Rq [DEC]

INTRODUCTION

Acoustic time-reversal mirrors are devices able to generate the time-reversed counterpart of a given wave, usually emitted by a point-like source.[1–3] This is done by measuring the incident acoustic field over a large surface, using an array of piezoelectric transducers. The signal of each channel is recorded, time-reversed, and finally re-emitted by the same element. This process creates a wave with the same shape as the incident one, but propagating in the opposite direction, thus focusing on the location of the initial source. One of the main problems of acoustic time-reversal experiments is the need of independent transmit/receive channels for every transducer element. A reduction of the number of elements generally implies a smaller aperture, and thus larger focal spots. In several experiments, it has been observed that multiple reflections and scattering tend to enhance focusing quality in resolution and amplitude. Roux *et al.*[6] carried out time-reversal experiments in waveguides: The reflections on the boundary artificially enlarge the aperture of the time-reversal mirror and thus reduce the focal spot size. Derode *et al.*[7] performed time-reversal experiments through multiply scattering media. Besides the surprising temporal recompression of the reversed signals, the focal spot size corresponds more closely to an aperture associated with the size of the multiple scattering medium rather than to the physical aperture of the mirror itself. In both cases, the information contained in the wider angles, which is lost for small apertures, is redirected or scattered onto the active surface of the mirror, which thus may be reduced. The price to pay for this gain of information is a longer recording time for the signal.

In this study, we examine the reduction of the receivers down to one. In this case, the propagation medium has to be a closed cavity to avoid information loss at infinity, with very weak absorption to allow recording over a long period of time. We have chosen a 2-D silicon wafer as the propagation medium; waves are injected and measured by transversal transducers, fixed to aluminum cones. It will be shown that our measurements are consistent with the hypothesis that the shape of the cavity is of crucial importance. In fact, we use a cavity with chaotic ray dynamics: The information contained in each ray emitted by the source can only be recorded if the ray, after several reflections, passes sufficiently near the time-reversal transducer. This behavior is ensured by ergodicity, which can be easily obtained by choosing a cavity in the shape of a *chaotic billiard*. Such a cavity also ensures mixing of the ray angles.

However, we have to point out one fundamental difference of this setup as compared with the experiments cited above. This is no longer a scattering experiment where we measure the outgoing waves after scattering from the medium. In the closed cavity, we measure instead the wave field at some given point inside the medium. Thus, unlike in scattering experiments, the wavefronts here continue to propagate in the medium after being measured and may even be measured again after several reflections at the boundary. This possibility of a multiple measurement is a disadvantage; it will be shown that it ultimately leads to a reduction of the quality of the time-reversed wave field.

In Sec. I, we present the general characteristics of our experimental setup. Section II shows how one-channel time-reversal experiments are carried out, and presents the spatial and temporal focusing properties. It turns out that the focusing quality increases with the length of the reversed signal. Section III describes this growth by a statistical approach of the ray dynamics of the cavity. Section IV gives two examples of cavities, where the assumption of ergodicity is not fulfilled, and the time-reversal process fails to work properly.

[a]Current affiliation: Department of Electrical Engineering, University of Rochester, Rochester, NY 14627. Electronic mail: draeger@ee.rochester.edu

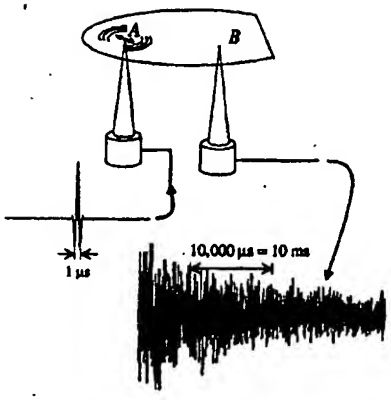

FIG. 1. Elastic waves are injected by means of transversal transducers fixed to Al-cones. A short signal, injected at one of the transducers, A, creates a long-lasting, reverberating wave field: The signal obtained at a second point, B, is slowly decaying.

I. EXPERIMENTAL SETUP AND SYSTEM PROPERTIES

The propagation media we use are circular wafers of 100- or 125-mm diameter, with a segment of variable size cut off (between 4% and 75% of the diameter). A billiard of the same shape has been shown to have chaotic trajectories.[8] The wafers are 525 μm thick and cut parallel to the plane (100) of the crystal lattice. If we neglect anisotropy, only three modes of propagation exist in the frequency range we used (around 1 MHz): *SH* waves with a nondispersive velocity around 5000 m/s, the Lamb mode S_0 with approximately 8300 m/s, and the highly dispersive A_0 mode with respective phase and group velocity of 2600 ± 100 m/s and 4400 ± 200 m/s. During the typical scale of time (1 ms) of an experiment, the waves are reflected between 40 and 80 times at the boundary. The *SH* and S_0 waves are coupled by reflections at the border of the cavity; the A_0 mode propagates independently. Besides, the A_0 propagation is isotropic in the plane. While, by definition, the *SH* mode has no normal surface displacement, this displacement of the S_0 mode is only very weak, as this mode is quasilongitudinal in the frequency range we use. The A_0 mode, being quasitransversal, is the only mode having sufficient normal surface displacements to be detected by an optical interferometer. This mode also has stronger coupling to the surrounding air, which results in a higher decay rate.

Sound injection and measurement is done by transversal transducers fixed to Al cones whose tips touch the wafer (Fig. 1). This technology has initially been developed by J.-P. Nikolovsky in our school for sound injection in glass plates.[9] It permits a point-like coupling to the system with negligible perturbation of the wave field. The tip of the cone acts as a dipole source and/or measuring point. The A_0 and S_0 waves are mainly emitted in directions around the polarization axis x, and the *SH* waves travel in the perpendicular directions (Fig. 2). It turns out that the use of a dipole source is not the best choice as it permits *a priori* only dipole focusing in time-reversal experiments. However, using a trick, we show in Sec. II how it is possible to obtain monopole focusing. Also, in Sec. IV, we point out how the use of a dipole source reveals interesting aspects of the chaotic behavior of the medium.

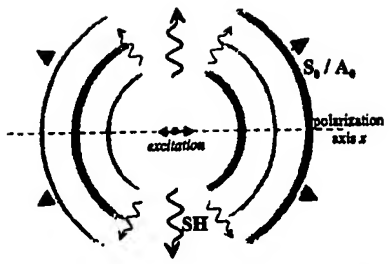

FIG. 2. The modes S_0 and A_0 are mostly emitted in directions around the polarization axis x of the dipole source point, the *SH* waves mainly in the perpendicular directions.

Injection of a short pulse in one of the transducers, A, creates inside the cavity a reverberating acoustic field with weak attenuation. In fact, the signal observed (after preamplification) by a second transducer, B, is slowly decaying (Fig. 1) with a decay period thousands of times longer than the injected signal (1 μs). Figure 3 shows the intensity decay on a logarithmic scale. One observes indeed two different regimes: During the first few milliseconds, the mode A_0 dominates, but decreases relatively quickly with a period of approximately 3 ms, thus revealing the slow decay of the coupled S_0/SH waves (10 to 20 ms, depending on the wafer's size). The length of the signals to be time-reversed (the time-reversal windows) is, with a maximum of 2 ms, always small compared to the latter decay period, and the intensity level inside the window will be considered as constant in the regime S_0/SH. For experiments involving the A_0 mode, we give only qualitative results.

The electronics of the time-reversal mirror provide for the initial emission a short sinusoidal burst of 1 MHz central frequency and a Gaussian envelope of width 0.4 μs, with an

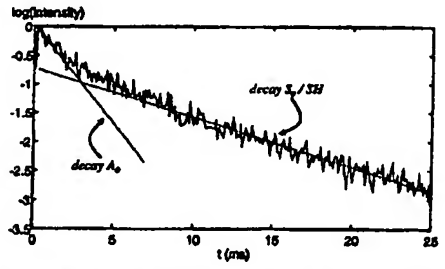

FIG. 3. Decay of the average intensity received at point B after injection of a short signal in A. For relatively short propagation times, the Lamb mode A_0 dominates. But as this mode is better coupled to the surrounding air, it decreases more quickly than the S_0 and *SH* modes that are permanently converted into each other at the boundary.

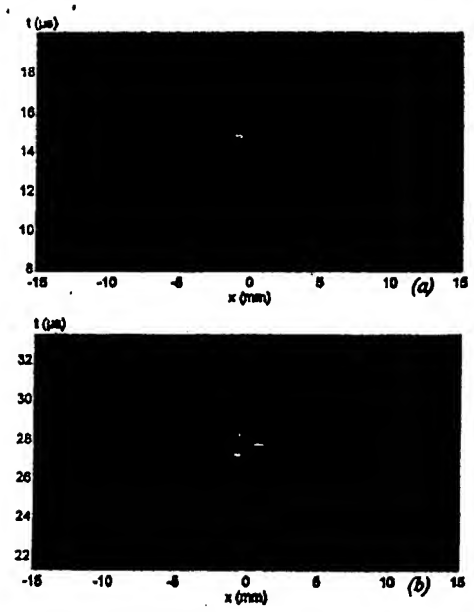

FIG. 4. B-scans of the normal surface displacement as measured with an optical interferometer along the polarization axis x of the dipole source A (at $x=0$), (a) during the initial emission, (b) during refocusing. The B-scans have been obtained using a spatial step of 0.1 mm and a sampling frequency of 15 MHz.

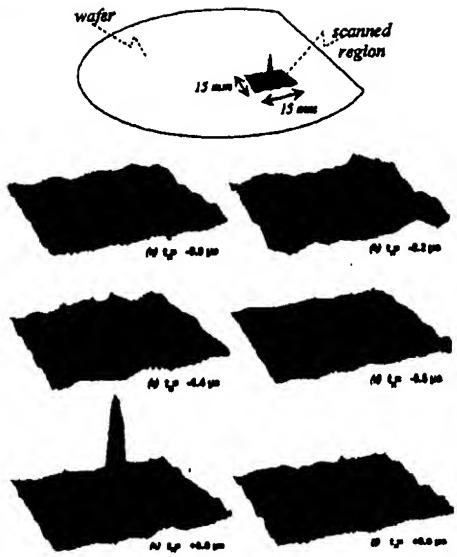

FIG. 5. Linear representation of the monopole refocusing A_0 wave, measured by the interferometer. Note the circular shape of the wavefronts and the background noise level, best seen in (a): One-channel time-reversal produces excellent, but not perfect, results.

amplitude between 10 and 80 V into a 50-Ω impedance. The received signals are digitized using 8 bits with a sampling frequency of either 7.5, 10, or 15 MHz.

II. THE TIME-REVERSAL EXPERIMENT

In the first step of the experiment, the transducer at A emits a short pulse at $t=0$. At point B, the signal is recorded and, after time-reversal and amplification, a part $\Delta T=[t_1,t_2]$ (the time-reversal window) is reinjected at this same point during the second step. Using a new (simply shifted) variable of the time scale t_R, we start re-emission at $t_R=-t_2$. This leads to a focusing in A at $t_R=0$.

A. Spatial recompression

We used a heterodyne Mach–Zehnder type of interferometer that was developed in our laboratory by D. Royer[10] to scan the acoustic field of the A_0 wave around the point A. The wafer is, in this case, mounted on a set of two motors able to translate the system in two dimensions, parallel to its surface. The emission is then repeated for every point where the time variation of the field is to be recorded. Figure 4(b) shows a B-scan of the normal surface displacement on the polarization axis x of A after a time-reversal of 1.5 ms in B. It has to be compared to the direct emission of the short pulse in A, shown in Fig. 4(a). In both figures, one observes the dipole character. However, if the B-scan of (b) was the real time-reversal of (a), there should be no outgoing wave after focusing. This is a common property of all time-reversal experiments: The energy in the system is not sucked out at the moment of focusing (which would be the time-reversal of the initial energy injection), so that the wave diverges again afterwards. Also, one can see some noise level elsewhere than the converging and diverging wavefronts. In summary, Fig. 4(a) and (b) show that it is possible to obtain a good, but not perfect, time-reversal with a one-channel time-reversal in B. But for a quantitative evaluation, a monopole focusing is preferable.

We have used a trick to obtain a monopole focal spot using transversal transducers. In the first step, the short pulse is now injected by the transducer at B instead of A. Instead of the second transducer, we use the interferometer to record the signal at point A. Being sensitive to normal surface displacements, the interferometer acts as a monopole receiver. The reciprocity principle tells us that the signal obtained is exactly the same as the one that would be recorded with a monopole emitter in A and a dipole receiver in B. Thus, this signal can be used to simulate a time-reversal experiment with a monopole source at A and a dipole reversal point at B. In the second step, we reinject a part of the signal at B. This leads to a monopole focusing at A. A linear representation of the A_0 wave field around the focal spot is given in Fig. 5. It has been measured on a square of 15×15 mm with a step of 0.25 mm for a time-reversal window of size 2 ms. One observes circular incoming wavefronts which focus at $t_R=0$ in

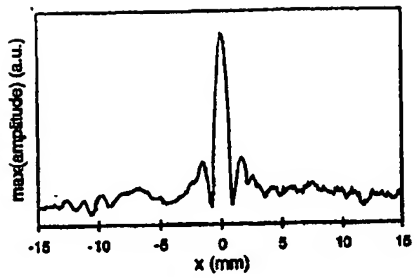

FIG. 6. Cut through the focal spot.

A. This means that in a closed reflecting medium, using a single emission point (the reversal point B), it is possible to obtain a focusing quality which corresponds to an angular aperture of 360°. But there is a certain noise level inside the system. This shows that the spatial recompression of the time-reversal process is less than perfect far from the focus. However, the cut through the focal spot, shown in Fig. 6, has a width of 1.1 mm for a central wavelength of 2.6 mm. This indicates that the A_0 wave is almost perfectly focused near the peak.

B. Temporal recompression

Again using transducers for both A and B, we now observe the refocused signal at A after time-reversal at B. One obtains a sharp peak at $t_R=0$, standing out from more or less temporal sidelobes (Fig. 7). If we change the position of the time-reversal window, the peak does not change in shape or amplitude, unlike the sidelobes (Figs. 8). As the medium is linear, the signal obtained by a reversal of a long window (which can be cut into several small windows) is the same as the superposition of the contributions of all the small windows. This implies that the amplitude of the peak increases linearly with ΔT (which stands, depending on the context, for the interval $[t_1,t_2]$ of the time-reversal window or, as here, for its length). It means also that higher amplitudes at the focus can be obtained not only by emission of a stronger, but also with a longer, signal. Excluding the possibility of a destructive superposition of the (temporal) sidelobes, their rms value increases linearly with $\sqrt{\Delta T}$ if the contributions of different windows are perfectly uncorrelated, or faster if they are not.

In Fig. 9, we present refocused signals for different window sizes, and, in Fig. 10, the peak/sidelobe intensity ratio. From a certain value of ΔT on (about 1 ms), the shape of the sidelobes does not seem to change any more. The intensity ratio, which increases linearly for small ΔT, saturates for

FIG. 7. Refocused signal obtained at A after a time-reversal of 1600 μs at B. The presented signal is about 210 μs long.

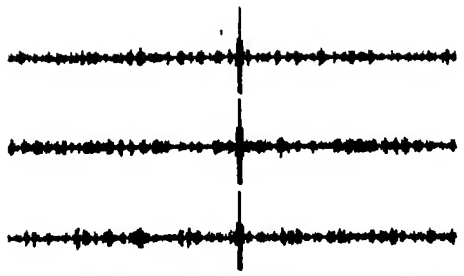

FIG. 8. Refocused signals for different time-reversal windows of same size (120 μs). The sidelobes change, but the peak is not altered.

high values. The refocused signal $s_{\Delta T}(t_R)$ approaches then an asymptotic shape, $S_\infty(t_R)$, and increases linearly with ΔT: $s_{\Delta T}(t_R)\approx\Delta T\cdot S_\infty(t_R)$, for $\Delta T\to\infty$. In particular, for large time-reversal windows, the refocused signal does not depend on their position, but only on their length. We consider the refocused signal $s_{\Delta T}(t_R)$ as a superposition of two contributions: A first part, $\Delta T\cdot S_\infty(t_R)$, which does not change in shape and which contains the peak as well as certain unavoidable sidelobes, called *residual sidelobes*. The

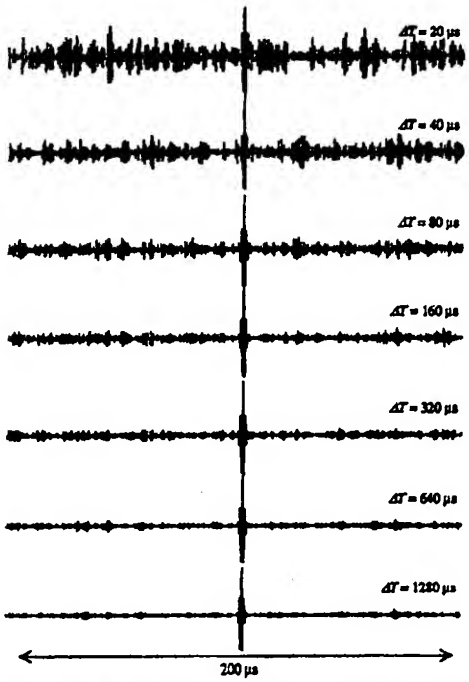

FIG. 9. Refocused signals for different time-reversal window sizes. The quality of the focus increases with the size. (Each amplitude has been normalized by a division by ΔT.)

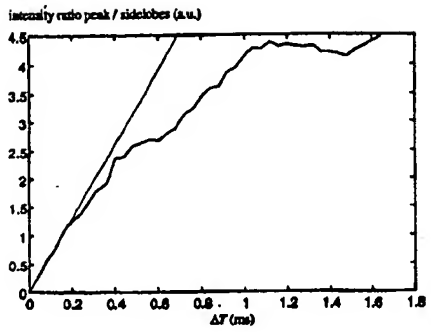

FIG. 10. For small time-reversal window sizes, the peak/sidelobe intensity ratio increases linearly, but enters a saturation regime for longer reversed signals.

second part changes with position and size of the window and can hence be reduced by reversing a longer signal. We designate it *noise*: $s_{\Delta T}(t_R)=\Delta T\cdot S_\infty(t_R)+$noise. This noise is not a measurement noise that can be reduced by averaging over several acquisitions. On the contrary, this noise is reproducible from one acquisition to the other; its origin is only in the limited size of the time-reversal window.

III. THE RAY MODEL

A. Introduction

In this section, we propose a simple statistical approach to explain the noise appearance. It is inspired by ray trajectories inside the cavity. The description of the wave field by a ray approximation is mostly intuitive and even difficult to justify as the radius of curvature of the cavity is relatively small and the paths are long. However, as we shall see, it fits exactly the experimental observations of the signal-to-noise ratio. The main idea is the following: In the first step of the experiment, imagine that A emits acoustic rays in all directions. (For simplicity, let A and B be monopole sources/receivers and the short pulse be a δ-function.) As the cavity is ergodic, every ray passes after more or less reflections sufficiently near B to be measured. The signal obtained is then a series of pulses, each one corresponding to a particular path between A and B. In the second step, a part of this signal is time-reversed and reinjected at B. Unlike a time-reversal mirror that creates the reversed wavefront in front of its active surface, B does not send back each peak only in the direction where the corresponding ray came from, but in all directions. Rays taking the "good" direction trace exactly their path back and arrive at $t_R=0$ at A. At this point, they superpose in a constructive way, giving the refocusing peak. All the rays taking "bad" directions may also superpose, thus giving rise to noise. But their superposition may be considered as random, thus increasing more slowly with the length of the time-reversal window than the refocusing peak: The signal-to-noise ratio is higher for longer reversed signals.

B. Calculation of the signal-to-noise ratio

Let $h(t)=h_{AB}(t)=h_{BA}(t)$ be the impulse response from A to B. Imagine that $h(t)$ is a superposition of Dirac pulses with arrival time t_i and amplitude A_i:

$$h(t)=\sum_i A_i\delta(t-t_i).$$

[This assumption is not strictly true as, in 2D, the impulse response is *not* giving δ-peaks, but peaks of type $H(t-r/c)\cdot(t^2-r^2/c^2)^{-1/2}$, where H is the Heaviside step function, r the distance and c the wave speed. However, for long distances and short pulses, the only effect of the different impulse response is a change in shape of the received signal, which can be formally included in the excitation function $f(t)$ emitted by A that convolves finally the impulse response.]

We define $\rho(t)=\langle\Sigma_i\delta(t-t_i)\rangle$ as the average density of ray arrival times. The brackets $\langle.\rangle$ are defined as an ensemble average over all possible pairs of points (A,B). Of course, the impulse response is different for every pair of points, but because of the ergodic character of the cavity, we expect the same statistical properties. Let $\overline{A}(t)=\langle A(t)\rangle$ denote the average amplitude as a function of time, and $\overline{A^2}(t)=\langle A^2(t)\rangle$ denote the average of its square. As excitation signal $f(t)$, we take a short pulse centered around $t=0$ and with $\int dt\, f(t)=0$, i.e., of average zero. The signal measured at B is then

$$S_{AB}(t)=h(t)*f(t)=\sum_i A_i f(t-t_i)$$

and its expectation value is

$$\langle S_{AB}(t)\rangle=\int dt_i\,\rho(t_i)\overline{A}(t_i)f(t-t_i).$$

We assume that $\rho\overline{A}$ varies slowly enough during the duration of f so that the integral vanishes: $\langle S_{AB}(t)\rangle=0$.

We reinject a part of the signal $\Delta T=[t_1,t_2]$ in B. The part of the reversed impulse response is

$$h^{\Delta T}(-t_R)=\begin{cases}h(-t_R), & t_R\in[-t_2,-t_1]\\ 0, & \text{elsewhere}\end{cases}.$$

Due to reciprocity, the impulse response from B to A is the same as the one from A to B, and we obtain for the signal at A after reversal in B (for $\Delta T\gg$width of f)

$$S_R(t_R)=f(t_R)*(h^{\Delta T}(-t_R)*h(t))$$

$$=f(t_R)*\int_{\Delta T}d\tau\,h(\tau)h(t_R+\tau).$$

As h is a Dirac function for every arrival time, $h(\tau)h(t_R+\tau)$ is nonzero if and only if τ and $t_R+\tau$ correspond to two arrival times. Let $t_i=\tau$ and $t_j=t_R+\tau=t_R+t_i$, then the signal can be written

$$S_R(t_R)=\sum_{t_i\in\Delta T}\sum_{t_j}A_iA_jf(t_R-(t_j-t_i)).$$

Hence, the refocused signal is a superposition of many elementary signals $f(t)$. We are going to split this sum into

three parts. The first one, responsible for the refocusing peak at $t_R=0$, is given by $t_i=t_j$, i.e., the diagonal elements of the double sum:

$$S_{\text{peak}}(t_R)=f(t_R)\sum_{t_i\in\Delta T}A_i^2.$$

The second part can be evaluated by assuming a random superposition of the elementary signals, given by all pairs (t_i,t_j) whose difference behaves as a random variable. We call them *uncorrelated pairs* (t_i,t_j) and the corresponding part of the signal *incoherent noise*.

$$S_{\text{noise}}(t_R)=\sum_{\substack{t_i\in\Delta T\\ t_i\neq t_j\text{uncorr.}}}A_iA_jf(t_R-(t_j-t_i)).$$

This sum contains almost all pairs of arrival times. But there are also pairs $t_i\neq t_j$ that are correlated. This fact can be ascribed to rays that, with origin at A, pass over this same point before arriving at B and to rays passing over B several times during propagation. These pairs give rise to the residual sidelobes, the third part of the sum:

$$S_{\substack{\text{residual}\\ \text{sidelobes}}}(t_R)=\sum_{\substack{t_i\in\Delta T\\ t_i\neq t_j\text{corr.}}}A_iA_jf(t_R-(t_j-t_i)).$$

The latter sum cannot be evaluated *as is*; the residual sidelobes are not described in a satisfactory way by our ray model. However, a model using a decomposition of the wave field in eigenmodes of the cavity gives a complete description of this phenomenon. It is published in a second paper.[11]

Now we want to evaluate the signal-to-noise ratio, i.e., the peak-to-noise ratio.

The expectation value of the peak is

$$\langle S_{\text{peak}}(t_R)\rangle=f(t_R)\int_{\Delta T}dt_i\,\rho(t_i)\overline{A^2}(t_i).$$

The expression $\rho\overline{A^2}=I_0$ represents the average intensity measured in B during the first step. Assuming an ergodic lossless cavity, its value must be constant in time, thus

$$\langle S_{\text{peak}}(t_R)\rangle=f(t_R)I_0\Delta T.$$

The amplitude of the peak is proportional to the excitation function and the window size ΔT. It does not depend on the density of arrival times or the corresponding amplitudes. The incoherent noise is, of course, of average zero. Its variance is given by

$$\langle S_{\text{noise}}^2(t_R)\rangle=\left\langle\sum_{\substack{t_i\in\Delta T\\ t_i\neq t_j\text{uncorr.}}}A_iA_jf(t_R-(t_j-t_i))\sum_{\substack{t_i'\in\Delta T\\ t_i'\neq t_j'\text{uncorr.}}}A_{i'}A_{j'}f(t_R-(t_j'-t_i'))\right\rangle$$

$$=\left\langle\sum_{\substack{t_i\in\Delta T\\ t_i\neq t_j\text{uncorr.}}}A_i^2A_j^2f^2(t_R-(t_j-t_i))\right\rangle+\left\langle\sum_{\substack{t_i\in\Delta T\\ t_i\neq t_j\text{uncorr.}}}A_iA_jf(t_R-(t_j-t_i))\sum_{\substack{t_i'\in\Delta T\\ t_i'\neq t_i,t_j'\neq t_j\\ t_i'\neq t_j'\text{uncorr.}}}A_{i'}A_{j'}f(t_R-(t_j'-t_i'))\right\rangle.$$

In these sums, several terms are excluded corresponding to correlated or same-arrival times. As these terms are small in number compared to the other ones, we commit only a small error by reintroducing them, but supposing them uncorrelated. The average of the double-sum terms can then be changed to a product of two averages, in which each factor is equal to the noise average $\langle S_{\text{noise}}(t_R)\rangle$ that is zero. The only contribution is given by the diagonal terms. Thus,

$$\langle S_{\text{noise}}^2(t_R)\rangle=\int_{\Delta T}dt_i\int dt_j\,\rho(t_i)\overline{A^2}(t_i)\rho(t_j)\overline{A^2}(t_j)\times f^2(t_R-(t_j-t_i)).$$

We replace $\rho\overline{A^2}$ by I_0. The integral over t_j simplifies to $E_f=\int dt\,f^2(t)$, the "energy" of the excitation function. One obtains finally

$$\langle S_{\text{noise}}^2\rangle=E_fI_0^2\Delta T,$$

independent from t_R.

The peak-to-noise ratio is found to be

$$R_{\text{p/n}}=\max\langle S_{\text{peak}}(t_R)\rangle/\sqrt{\langle S_{\text{noise}}^2\rangle}=(\max(f(t))/\sqrt{E_f})\sqrt{\Delta T},$$

which is proportional to the square root of ΔT. Thus, a short signal of high amplitude is better suited for high signal-to-noise ratios than a longer signal with a lower peak value, but containing the same energy.

C. Comparison with experiments

The signal-to-noise ratio calculated above is not convenient for the description of experimental data. First, we prefer a value which does not depend on the shape of the signal. We consider, therefore, the energy of the peak instead of its maximum:

$$E_{\text{peak}}^{\text{exp}}=\int dt_R\,S_{\text{peak}}^2(t_R);$$

$$E_{\text{peak}}^{\text{theory}}=\int dt_R\langle S_{\text{peak}}^2(t_R)\rangle=E_fI_0^2\Delta T^2.$$

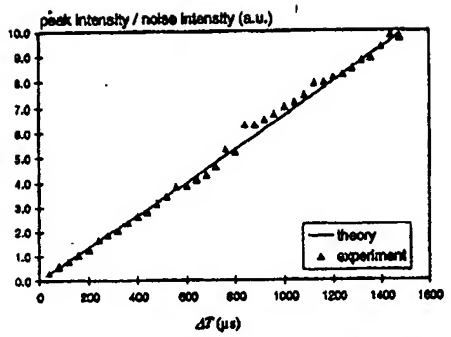

FIG. 11. Evolution of the peak/noise intensity ratio (after subtraction of the residual sidelobes) for increasing time-reversal windows.

Second, as we cannot directly measure the variance of the noise, we estimate its value by taking the average over a window Δt_R in the refocused signal. (Given the ergodic character of the system, this should be a good estimator.) The energy of the noise inside this interval is given by

$$E_{\text{noise}}^{\text{exp}} = \int_{\Delta t_R} dt_R \, S_{\text{noise}}^2(t_R);$$

$$E_{\text{noise}}^{\text{theory}} = \int_{\Delta t_R} dt_R (S_{\text{noise}}^2) = E_f I_0^2 \Delta T \Delta t_R .$$

The theoretical ratio is linear in ΔT:

$$E_{\text{peak}}^{\text{theory}} / E_{\text{noise}}^{\text{theory}} = \Delta T / \Delta t_R .$$

Third, we do not have direct access to the incoherent noise as it is superposed to the residual sidelobes. However, the difference of two refocused signals, $S_{\Delta T_1} - S_{\Delta T_2}$, for two nonoverlapping time-reversal windows ΔT_1 and ΔT_2 of the same size, erases the peak and the residual sidelobes. The noise behaves like a refocused signal obtained by a window of size $\Delta T = \Delta T_1 + \Delta T_2$. These facts have been taken into account to obtain the experimental data in Fig. 11. The agreement is excellent. Note that the straight line is the theoretical ratio, drawn without fit to the experimental data. This justifies thus, *a posteriori*, the model.

IV. TIME-REVERSAL IN REGULAR CAVITIES

In order to show the importance of the ergodic and mixing character of the cavity, we present here two examples of cavities, where this assumption is not, or not completely, fulfilled.

A. Rectangular cavities

Rectangles are a favorite example of regular billiards. The angle of the trajectory is a constant of motion and so the path of a ray can be predicted in the long term. By symmetry considerations, it is easy to see that a one-channel time-reversal in a rectangular cavity produces several focal spots other than the source point A, with different amplitudes. (In fact, there are up to nine.) In the experimental setup shown in

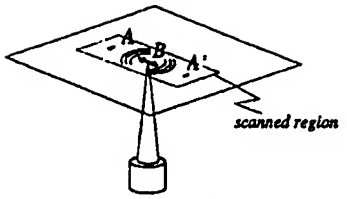

FIG. 12. One-channel time-reversal in rectangular cavities produces several focal spots. In this particular configuration (A located on the polarization axis of B, which is parallel to one side of the rectangle), some of them are superposed in A'.

Fig. 12, some of these image points superpose at A'. Figure 13 presents a C-scan, taken at the focusing instant, showing the monopole at A and its image at A', symmetrical to the reversal point B. The fact that B is a dipole source gives another interesting aspect to this experiment: B is only able to emit or receive in directions around its polarization axis. As the angle of each ray is conserved, the monopole focal spots at A and A' no longer have circular symmetry, but are biased by the directivity pattern of the reversal point.

B. Temporal dependence of mixing

Chaotic cavities whose shape is only slightly different from the regular case do not reveal their ergodic properties over short time-scales. For the C-scans presented in Fig. 14, we have used an almost circular wafer, with a segment of only 4% of the diameter cut off. In circular billiards, the constant of motion is the angular momentum. If A and B are at the same distance from the center, this would lead, just as in the case of rectangular billiards, to monopole focal spots with the directivity pattern of the dipole reversal point. In the case of our almost regular cavity, the time-reversal of the first 2 ms ($\Delta T = [0;2\text{ ms}]$) shows exactly this behavior [Fig. 14(a)]. If one reverses instead the following two milliseconds ($\Delta T = [2\text{ ms};4\text{ ms}]$), the focal spot is of circular symmetry [Fig. 14(b)]. Obviously, the angular momentum of a ray is conserved over medium periods of time. To be mixed, the ray has to be reflected at least once at the small part of the boundary where the segment is cut off. And only a mixing of the angular momenta allows rays to approach the focal spot from other sides than the directivity pattern of the reversal point.

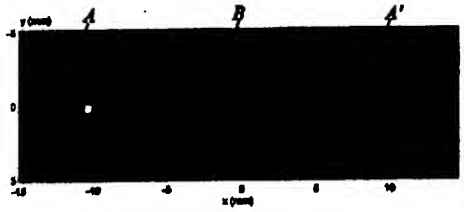

FIG. 13. C-scan of two (monopole) focal spots in a rectangular cavity as measured by an optical interferometer. The converging wavefronts are no more circular, but biased by the directivity pattern at the reversal point B.

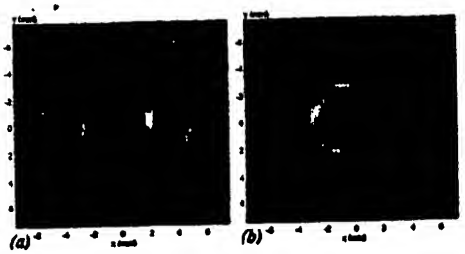

FIG. 14. C-scans of the refocused waves in a weakly chaotic billiard. (a) Time-reversal of a window directly after emission (ΔT=[0,2000 μs]) still shows the directivity pattern of the reversal point. (b) Ray angles mix after longer trajectories (ΔT=[2000 μs,4000 μs]) and arrive from all directions at the focal spot.

V. CONCLUSION

Acoustic time-reversal experiments usually need large arrays of transducers. In this paper, we present experiments proving the possibility of reducing the number of elements down to one by using multiple reflections inside the propagation medium. The experiments are carried out with a 2-D silicon wafer, wherein the injection of a short ultrasonic pulse at one point reverberates over a very long time. The signal is recorded at a second point, time-reversed and re-emitted. We obtain an excellent focusing at the initial source location.

The focusing peak has been observed using two methods: First, we scanned the field of one propagation mode (A_0) around the focal spot using an optical interferometer. One is able to obtain circular converging wavefronts that collapse at the initial source point and diverge afterwards. However, a certain noise level cannot be avoided. Second, we observe the refocused signal using the transducer located at the initial source. We obtain a short peak standing out from more-or-less temporal sidelobes. The refocused signal depends crucially on the size of the time-reversal window, i.e., the length of the reversed signal. The amplitude of the peak increases linearly with the reversed time; the peak to sidelobes level improves. For long time-reversal windows, a saturation regime is entered where the sidelobes can no more be reduced. The increase of the focusing quality with the reversed time can be successfully described by a simple statistical model, inspired by ray trajectories inside the cavity. However, the residual sidelobes are not taken into account by this model. A more rigorous analysis, based on an eigenmode decomposition of the wave field, explains this phenomenon and is presented in a second paper dealing with the theoretical limits of the time-reversal process.[11]

The use of a chaotic cavity is of crucial interest. First, its ergodic ray dynamics ensures that every ray emitted by the source point can be recorded by the reversal point. Second, we give examples of regular cavities wherein the one-channel time-reversal does not work properly. Third, a theoretical analysis, given in another paper, also takes advantage by assuming some properties of chaotic wave billiards such as, for example, spectral rigidity. While classical chaos inhibits time-reversal experiments due to strong sensitivity to initial conditions, the wave chaos of this case is actually useful.

One-channel time-reversal experiments can be easily reproduced. Unlike usual time-reversal experiments which need, in general, up to 100 transducers and the corresponding independent transmit/receive electronics, one-channel experiments have an extremely simple and low-cost experimental setup. Only two transducers are needed, and one transmit and one receive channel. We used a 2-D cavity in our experiments, but a 3-D cavity should work as well.

Our lab is currently working towards a better characterization of the time-reversal experiments in the transition from regular to chaotic cavities. We also want to try waveguides with a cross section in the shape of a chaotic billiard to obtain time-reversed focusing using a time-reversal mirror with fewer transducer elements.

ACKNOWLEDGMENTS

The authors would like to thank J. P. Nikolovsky for the production of the Al-cones, D. Royer and J. L. Thomas for experimental help, and A. Derode for useful discussions.

[1] M. Fink, "Time-Reversal Acoustics," Phys. Today 50(3), 34–40 (1997).
[2] M. Fink, "Time-reversal of ultrasonic fields-Part I: Basic Principles," IEEE Trans. Ultrason. Ferroelectr. Freq. Control 39, 555–566 (1992).
[3] F. Wu, J. L. Thomas, and M. Fink, "Time-reversal of ultrasonic fields-Part II: Experimental Results," IEEE Trans. Ultrason. Ferroelectr. Freq. Control 39, 567–578 (1992).
[4] D. Cassereau and M. Fink, "Time-reversal of ultrasonic fields-Part III: Theory of the closed time-reversal cavity," IEEE Trans. Ultrason. Ferroelectr. Freq. Control 39, 579–592 (1992).
[5] D. Cassereau and M. Fink, "Focusing with plane time-reversal mirrors: An efficient alternative to closed cavities," J. Acoust. Soc. Am. 94, 2373–2386 (1993).
[6] P. Roux, B. Roman, and M. Fink, "Time-reversal in an ultrasonic waveguide," Appl. Phys. Lett. 70(14), 1811–1813 (1997).
[7] A. Derode, P. Roux, and M. Fink, "Robust Acoustic Time Reversal with High-Order Multiple Scattering," Phys. Rev. Lett. 75(23), 4206–4209 (1995).
[8] L. A. Bunimovitch, "On the ergodic properties of nowhere dispersing billards," Commun. Math. Phys. 65, 295–312 (1979).
[9] J. P. Nikolovsky and D. Royer, "Local and selective detection of acoustic waves at the surface of a material," IEEE Ultrason. Symp. Proc. (1997).
[10] D. Royer and E. Dieulesaint, "Optical detection of sub-angström mechanical displacements," IEEE Ultrason. Symp. Proc., 527–530 (1986).
[11] C. Draeger and M. Fink, "One-channel time-reversal in chaotic cavities: Theoretical limits," J. Acoust. Soc. Am. 105, 611–617 (1999).